Mon. Not. R. Astron. Soc. **000**, 000–000 (0000) Printed 5 February 2008 (MN LATEX style file v1.4)

LISA double black holes: Dynamics in gaseous nuclear discs

Massimo Dotti[1], Monica Colpi[2], & Francesco Haardt[1]
[1] *Dipartimento di Fisica & Matematica, Universitá dell'Insubria, Via Valleggio 11, 22100 Como, Italy.*
[2] *Dipartimento di Fisica "G. Occhialini", Universitá di Milano–Bicocca, Piazza delle Scienze 3, 20100 Milano, Italy.*

5 February 2008

ABSTRACT

We study the inspiral of double black holes, with masses in the *LISA* window of detectability, orbiting inside a massive circum–nuclear, rotationally supported gaseous disc. Using high–resolution SPH simulations, we follow the black hole dynamics in the early phase when gas–dynamical friction acts on the black holes individually, and continue our simulation until they form a close binary. We find that in the early sinking the black holes lose memory of their initial orbital eccentricity if they co–rotate with the gaseous disc. As a consequence the massive black holes bind forming a binary with a low eccentricity, consistent with zero within our numerical resolution limit. The cause of circularization resides in the rotation present in the gaseous background where dynamical friction operates. Circularization may hinder gravitational waves from taking over and leading the binary to coalescence. In the case of counter–rotating orbits the initial eccentricity (if present) does not decrease, and the black holes may bind forming an eccentric binary. When dynamical friction has subsided, for equal mass black holes and regardless their initial eccentricity, angular momentum loss, driven by the gravitational torque exerted on the binary by surrounding gas, is nevertheless observable down to the smallest scale probed ($\simeq 1$ pc). In the case of unequal masses, dynamical friction remains efficient down to our resolution limit, and there is no sign of formation of any ellipsoidal gas distribution that may further harden the binary. During inspiral, gravitational capture of gas by the black holes occurs mainly along circular orbits: eccentric orbits imply high relative velocities and weak gravitational focusing. Thus, AGN activity may be excited during the black hole pairing process and double active nuclei may form when circularization is completed, on distance–scales of tens of parsecs.

Key words: Black Hole Physics: binaries, hydrodynamics – Galaxies: evolution, nuclei – Gravitational Waves – Quasar: general

1 INTRODUCTION

Today, we know that a tight link between the formation and evolution of galaxies and massive black holes (MBHs) exists. Black holes (BHs), with masses ranging from $\sim 10^6$ $M_\odot$ to 10^9 $M_\odot$ (e.g., Kormendy & Richstone 1995), are ubiquitous in the centre of nearby galaxies, and their masses show a tight correlation with the properties of the host stellar bulges (e.g., Magorrian et al. 1998, Gebhardt et al. 2000, Ferrarese & Merritt 2000, Häring & Rix 2004). If MBHs were also common in the past, and if galaxies merge as implied by hierarchical clustering models of structure formation, then massive black hole binaries (MBHBs) must have been formed in large number during the cosmic history.

Close MBHBs are natural, very powerful sources of gravitational radiation, whose emission is one of the major scientific targets of the next Laser Interferometer Space Antenna (*LISA*; see, e.g., Haehnelt 1994, Jaffe & Backer 2003, Sesana et al. 2005). The *LISA* interferometer (see Bender et al. 1994), sensitive in the frequency range between $10^{-5} - 10^{-1}$ Hz, will unveil, when in operation, MBHBs in the mass range $10^3\,M_\odot/(1+z) \lesssim M_{\rm BH} \lesssim 10^7\,M_\odot/(1+z)$: this mass window defines our "*LISA* black holes". The lighter objects ($10^{3-5}\,M_\odot/(1+z)$) are often referred to as intermediate mass BHs: their existence has been conjectured in the framework of hierarchical models of structure formation (e.g., Volonteri, Haardt & Madau 2003), and, recently, gained observational support (van der Marel et al. 2002 for a review, Gebhardt, Rich & Ho 2002, Colpi, Possenti & Gualandris 2002, Gerssen et al. 2002, Gebhardt, Rich & Ho 2005, Miller & Colbert 2004). Higher mass *LISA* BHs are instead in the lower end of the observed mass distribution, and are the target of our study.

LISA will detect MBHBs only during the last of a com-

plex sequence of events that starts when the two MBHs are a few kpc far apart, and terminates when they reach sub–pc scales, i.e., the distance at which gravitational waves (GWs) ultimately drive the final coalescence. How can MBHs reach the GW emission regime? The overall scenario was first outlined by Begelman, Blandford & Rees (1980) in their study of the long–term evolution of BH pairs in dense stellar systems. They indicated three main processes for the loss of orbital energy and angular momentum: (a) dynamical friction against the stellar background acts initially on the BHs as individual masses, favoring their pairing; (b) MBHs eventually bind to form a binary when the stellar mass enclosed in the orbit becomes less than the total mass of the two MBHs. The resulting binary continues to harden via 3–body interactions with the surrounding stars until it reaches the separation at which GWs become dominant; (c) in the third, and last, phase, GW back—reaction shrinks the binary and, depending on the eccentricity and separation of the orbit, leads to coalescence. The dynamical range that a MBHB separation needs to cover to become a *LISA* source is enormous, more than six orders of magnitude.

Early studies have explored the pairing of MBHs in mergers of purely collisionless spherical halos (Makino & Ebisuzaki 1996, Milosavljević & Merritt 2001, Makino & Funato 2004). Governato, Colpi & Maraschi (1994) first noticed that when two equal mass halos merge, the MBHs inside their host nuclei are dragged toward the centre of the remnant galaxy, forming a close pair. The situation is different in unequal mass mergers, where the less massive halo is tidally disrupted, and leaves its MBH wandering in the outskirts of the main halo. Thus, depending on the mass ratio and internal structure of the halos and host galaxies, the transition from phase (a) to phase (b) can be prematurely aborted. Similarly, the transit from phase (b) to phase (c) is not always secured, as the stellar content of the "loss cone" may be not enough to drive the binary separation to the GW emission regime (see, e.g., Milosavljevic & Merritt 2001, Yu 2002, Berczik, Merritt & Spurzem 2005, Sesana, Haardt & Madau 2005, in preparation). In the studies cited above, the background was purely collisionless.

Since *LISA* BH coalescences are likely to be events associated with mergers of galactic structures at high redshifts, it is likely that their dynamics occurred in gas dominated backgrounds. So one might expect that phases (a) and (b) can be profoundly affected by the presence of a dissipative component. Mergers cause large–scale gas dynamical instabilities that lead to the gathering of cool gas deep in the potential well of the interacting systems dragging the BHs to the centre of the remnants.

Observations of interacting Luminous Infrared Galaxies (LIRG) in our local universe have provided evidence of the presence of huge amounts of cool atomic and molecular hydrogen collected in their cores (Sanders & Mirabel 1996). The total gas mass is typically $\sim 5\times10^9\,\mathrm{M}_\odot$, located in the rotationally supported disc in the inner ~ 100 pc (Downes & Solomon 1998). Interestingly, at least in three cases (NGC 6240, Arp 299 and Mkn 463) combined X–ray and infrared observation hint for the presence of two active MBHs in their nuclei (Hutchings & Neff 1988, Komossa et al. 2003, Ballo et al. 2004).

On theoretical ground, the advances in numerical computing allow to investigate in greater detail the process of BH pairing. Recently, Kazantzidis et al. (2005) explored the effect of gaseous dissipation in mergers between gas–rich disc galaxies with central BHs, using high resolution N–Body/SPH simulations. They found that the presence of a cool gaseous component is essential in order to bring the BH to close distances, since gas infall deepens the potential well, preserving the less massive galaxy against tidal disruption. Moreover, the interplay between strong gas inflows and star formation seems to lead naturally, in these mergers and regardless of the masses of the interacting galaxies, to the formation, around the two MBHs, of massive circum–nuclear gaseous discs on a scale ~ 100 pc, close to the numerical resolution limit. Yet, it is still difficult to establish the internal kinematic properties of the disc and of the MBH orbits, whether they are elongated or circular.

The work of Kazantzidis et al. (2005) and the observational evidence that discs are ubiquitous, have provided our main motivation to study the process of BH pairing in gaseous circum–nuclear discs. Escala et al. (2005, hereinafter ELCM05; see also Escala et al. 2004) have studied the role played by gas in affecting the dynamics of MBHs of equal masses (in a range of $5\times10^7\,\mathrm{M}_\odot \le M_{\rm BH} \le 2.5\times10^9\,\mathrm{M}_\odot$) moving on circular orbits in Mestel discs of varying clumpiness. They explored the decay across phase (a) controlled by dynamical friction and the transition to the regime (c) dominated by GW emission, highlighting the role played by gravitational torques in shrinking the binary. ELCM05 followed the orbital decay of a MBHB of total mass equal to $10^8\,\mathrm{M}_\odot$ down to 0.1 pc, just around the critical distance for the transition of the GW domain. The last phase of orbital decay in a gaseous enviroment has been studied by Armitage & Natarajan (2002), and by Milosavljevic & Phinney (2005). The first paper addresses the issue of black hole migration within a pre–exisiting Shakura & Sunayev (1973) accretion disc around a much heavier black hole. It is show how orbital angular momentum losses due to binary–gas interactions can shrink the orbit in $\sim 10^7$ yrs, down to a separation where GW emission rapidly leads the binary to coalescence. The authors suggest that an increased accretion rate during the migration is unlikely, while strong, potentially observable outflows should preceed the very last phase of the evolution. Milosavljevic & Phinney (2005) argued that, after coalescence, residual disc gas could fill the circum–binary gap, producing, within few years, an X–ray *LISA* afterglow.

Further studies are necessary. First, because *LISA* is designed to detect MBHBs lighter than the mass range explored by ELCM05, and, second, because, in hierarchical cosmologies, only mergers occurring at very high redshifts involve almost equal mass MBHBs, while, at later epochs, coalescences of unequal mass MBHBs are much more common (Volonteri et al. 2003). In the present work, we investigate the sinking process of *LISA* BHs inside a massive rotationally supported disc ($M_{\rm Disc}\sim 10^8\,\mathrm{M}_\odot$) having finite vertical extension. The disc is constructed starting from an initial Mestel distribution, and is allowed to relax into a new dynamical equilibrium. The BHs have equal and unequal masses and are moving initially on orbits of varying eccentricity: from circular to highly elongated, in order to reflect different conditions in their sinking from the kpc–distance scale down to the scale of the nuclear disc which they inhabit.

We would like to address a number of questions.

(i) How do eccentric orbits evolve? Do they become circular? This issue may be relevant in establishing the initial conditions for the braking of the binary (phase b) due to the slingshot mechanism and/or gaseous gravitational torque. Armitage & Natarajan (2005) have recently shown that a residual small (but non zero) eccentricity can be amplified by the binary–disc interaction before GW emission dominates.

(ii) During the sinking process, do the BHs collect substantial amounts of gas? This is a query related to the potential activity of a MBH during a merger and its detectability across the entire dynamical evolution.

(iii) When a binary forms, how gravitational torques, exerted by the surrounding gas, depend on the mass ratio between the two BHs? The possibility that the binary stalls has to be studied with more scrutiny and may also depend on the issue (i).

(iv) What mechanisms, besides this torque, can drive the binary into the GW dominated decaying phase? We consider the effects of BH mass growth on their dynamics in §5.

The paper is organized as follows. In section §2 we describe the numerical simulations we performed. Results concerning equal mass binaries are reported in §3, while in next §4 we describe unequal mass systems. Last §5 is devoted to discussion and conclusions.

2 N–BODY/SPH SIMULATIONS

The circum–nuclear region of a merger remnant is described here as a superposition of a spherical stellar spheroid and of an axisymmetric gaseous disc. The disc hosts two BHs treated as collisionless particles. The spheroidal component (bulge) is modeled initially as a Plummer sphere, while the disc as a Mestel distribution. We evolve the system using the N–Body/SPH code GADGET (Springel, Yoshida & White 2001).

2.1 Bulge and gaseous disc

The Plummer law for the stellar bulge density is

$$\rho(r) = \frac{3}{4\pi}\frac{M_{\rm Bulge}}{a^3}\left(1+\frac{r^2}{a^2}\right)^{-5/2}, \qquad (1)$$

where a is the core radius, r the radial coordinate, and $M_{\rm Bulge}$ the total mass of the spheroid.

The Mestel disc follows a surface density profile

$$\Sigma_{\rm Disc}(R) = \frac{\Sigma_0\, R_0}{R} \qquad (2)$$

where R is the radial distance, projected in the disc plane, and Σ_0 and R_0 reference values. The disc is rotationally supported and is characterized by a circular velocity $V_{\rm cir}$ independent of R, in the limit of infinitesimal thickness and low temperature. The bulge, introduced to stabilize the disc against gravitational instabilities, has a mass $M_{\rm Bulge} = 6.98 M_{\rm Disc}$.

In our current hydrodynamical simulations, the disc has finite radial extension $R_{\rm Disc} = 2a$, and finite vertical thickness Z_0 equal to a tenth of the disc radius $R_{\rm Disc}$. The vertical density profile is uniform, for a given R, initially. The total disc to bulge mass ratio inside $R_{\rm Disc}$ is 1:5. The units of the code are: [Mass]=$10^8\,{\rm M}_\odot$, [Time]=2.5×10^5 yr, [Length]=10.9 pc, [Velocity]=$41.5\,{\rm km\,s^{-1}}$, [Density]=$7.8\times10^4\,{\rm M}_\odot\,{\rm pc}^{-3}$. In these units $V_{\rm cir}=3.7$ (in the limit of zero disc thickness), and $G=21.9606$.

The equation of state for the gas in the disc is a polytrope,

$$P = K\rho^\gamma, \qquad (3)$$

where γ is equal to 5/3, corresponding to pure adiabatic evolution, and K is set equal to 2.3325, the value considered by ELCM05, for which the level of clumpiness during the evolution is minimized. In internal units $a=5$, $M_{\rm Bulge}=6.98$, $R_{\rm Disc}=10$, $M_{\rm Disc}=1$ and the sound speed of gas in the disc at $r=5$ is $c_s=(\partial P/\partial\rho)^{0.5}=0.289$, corresponding to a temperature of $T\simeq10^4K$. In our scheme we have not included the possibility that the gas develops a multiphase structure. This has been recognized as a relevant feature of self–gravitating discs (see, e.g., Wada & Norman 2001), and it is related to various feed–back mechanisms operating in realistic situations (e.g., star formation, radiative heating, shock induced cooling, etc.). Though a simple polytropic model, as the one we employed, does not catch the detailed thermodynamics of the gas, it is, nevertheless, an effective tool to study the orbital decay of MBHBs in self–gravitating discs (ELCM05).

In our simulations, the number of collisionless particles is 10^5, for the spheroid, while the number of gas/SPH particles is 235,331. With the above figures, our gas mass resolution is 100 times the mass of a single SPH particle, which is, in internal units, 4.25×10^{-6} ($425\,{\rm M}_\odot$ in physical units). The mass of bulge stars is 6.98×10^{-5} ($6980\,{\rm M}_\odot$), and the softening length is 0.1 (1.09 pc), equal for both type of particles.

Given these initial conditions, the collisionless spherical component, drawn from the Plummer phase–space distribution function, is in near equilibrium, while the disc, having finite thickness and homogeneous vertical density distribution is allowed to evolve into an equilibrium configuration along the R and z–axis. The disc is evolved for a dimensionless time of ~10 (2.6 Myrs) until the density and pressure fields find their equilibrium. Initially, the vertical collapse of the gas increases the pressure gradient in both vertical and horizontal directions, exciting small waves that propagate outwards. In settling toward equilibrium, Σ modifies and a small core forms in the central region, as shown in Figure 1 where we draw the initial (dashed line) and equilibrium (solid line) surface density profile; the gas density in the z direction becomes non uniform, when equilibrium is attained.

2.2 Black holes

The BHs are treated as collisionless particles and are placed in the disc plane. This is an assumption in agreement with the large scale simulation by Kazantzidis et al. (2005) who find that the BHs pair inside the massive circum–nuclear disc which forms in the remnant galaxy, on elongated orbits. We place our BHs on circular as well as rather eccentric orbits to bracket uncertainties.

We consider the case of *LISA* BHs with 1:1 ($10^6\,{\rm M}_\odot - 10^6\,{\rm M}_\odot$) and 5:1 ($5\times10^6\,{\rm M}_\odot - 10^6\,{\rm M}_\odot$) mass ratio. The

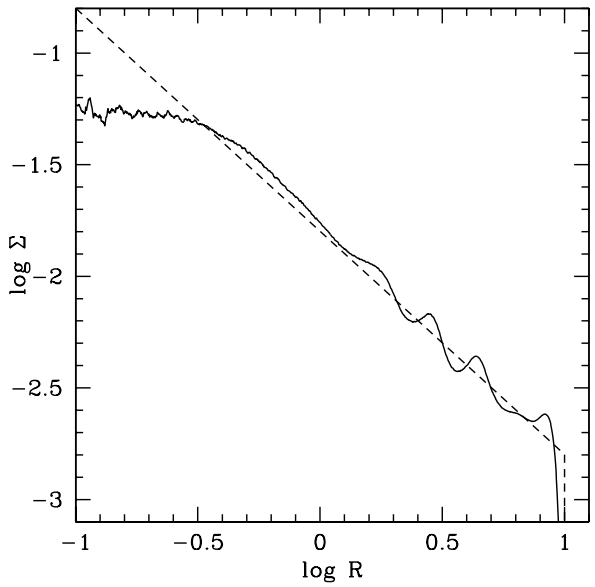

Figure 1. Surface density Σ as a function of the distance R from the centre of mass, in internal dimensionless units. The *dashed line* refers to the surface density of the Mestel disc, while the *solid line* describes the equilibrium profile after an elapsed time $\simeq 10$ (2.6 Myrs), corresponding to the initial condition of all our simulations.

FIGURE 2

Figure 2. Face–on projection of the disc for run A at time 2 Myrs. The color coding shows the z–averaged gas density, and the bright dots highlight the position of the two BHs that form prominent wakes behind their trails.

Table 1. Run parameters

run	$M^*_{\rm BH_1}$	$M^*_{\rm BH_2}$	$M^*_{\rm Disc}$	$M^*_{\rm Bulge}$	e
A	1	1	100	698	0
B	1	1	100	698	0.97
C	5	1	100	698	0
D	5	1	100	698	0.95
E	1	1	0	698	0.94
F**	5	1	100	698	0.95

* Masses are in units of $10^6\,{\rm M}_\odot$.
** $\rm BH_2$ in run F has a retrograde orbit.

softening of the collisionless BH particles is 0.1 (1.09 pc). In Table 1 we list the parameters used in our 6 simulations.

3 DYNAMICS OF EQUAL MASS BLACK HOLES

3.1 Circular Orbits

Run A is aimed to reproduce run D of ELCM05. Each *LISA* BH has a mass $M_{\rm BH} = 0.01 M_{\rm Disc}$ and is set on a circular prograde orbit inside the disc. The initial separation, relative to the centre of mass, is 5 (54.5 pc).

We plot in Figure 2 the density map of the gas surrounding the BHs at a selected time, to show the prominent over-densities that develop behind the holes causing their braking. The motion of the BHs is highly supersonic, and this explains the coherent structure and shape of their wakes (Ostriker 1999). Most of the disc gas lying out of BH orbits is somewhat "squeezed" into the wakes. Qualitatively, the extent of the wakes depends on the amount of disc mass perturbed by the orbiting BHs, which is a function of the BH masses.

Figure 3 shows the inspiral of the two BHs sinking because of dynamical friction mainly due to the gas component. The BHs evolve maintaining their orbits nearly circular until they reach the central, numerically unresolved, region. The time evolution of the BH relative separation $R_{\rm rel}$ is plotted in the inset of Fig. 3, and is in agreement with ELCM05.

Before reaching the force resolution limit, where integration stops, orbital decay becomes less efficient since the nature of the drag changes. Figure 4 gives, at late times, the mass in star and gas enclosed inside the sphere defined by $R_{\rm rel}$. When such mass is $\gtrsim 2\,M_{\rm BH}$, dynamical friction acts on the BHs as individual objects. At a time $t \simeq 8$ Myrs the mass drops below $2\,M_{\rm BH}$ and dynamical friction becomes inefficient. The BHs now are bound in a "binary", and the orbital decay proceeds further, but at a lower pace. This corresponds to the "transition regime" defined by ELCM05. Our resolution limit does not permit to test the subsequent "ellipsoidal regime" (ELCM05). We note that an ellipsoidal distribution of gas is already present when the binary is formed, as shown in Figure 8.

The BHs maintain a nearly circular orbit and this im-

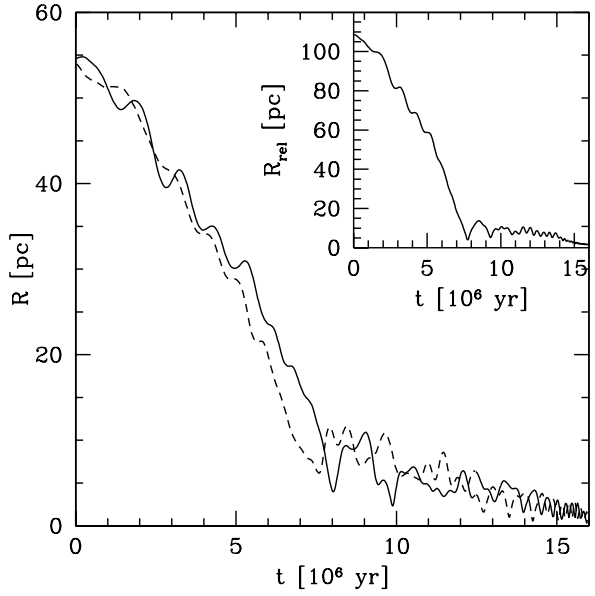

Figure 3. Distance R from the centre of mass, as a function of time t, for equal mass BHs in run A. *Solid* and *dashed* lines refer to the different BHs. The insert gives the BH relative separation $R_{\rm rel}$ versus time. Integration is halted when the resolution limit ($\simeq 1$ pc) is attained.

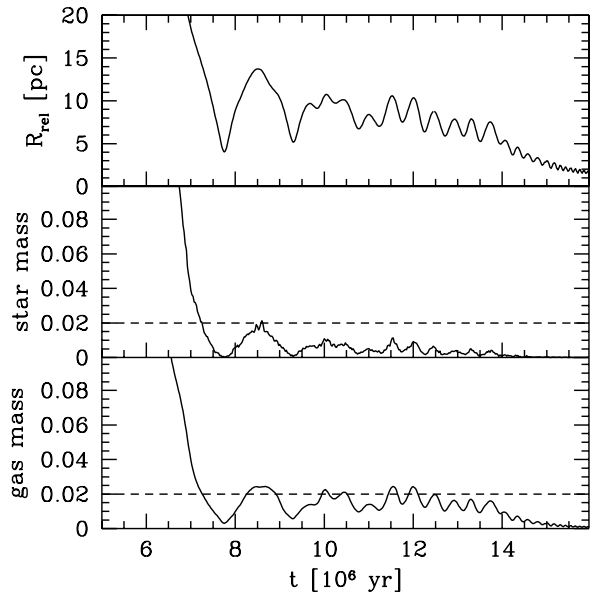

Figure 4. Upper panel: relative distance $R_{\rm rel}$ between the BHs versus time, for run A. Middle (lower) panel: mass (in internal units) in stars (gas) enclosed inside $R_{\rm rel}$, against time. Horizontal dashed lines indicate the total mass of the BHs.

plies that the relative velocity between the BHs and the rotationally supported gas particles is small. This suggests that some of the gas in the wake may become bound to the BHs while spiraling inwards. We find that the mass in gas particles associated to the over-density centred around each BH is $\sim 20\%$ of its mass, during inspiral. This number is calculated by summing the masses of all gas particles associated with a spherical density excess measured relative to the unperturbed disc, at the same position. This provides only an approximate estimate of the mass that can become bound to the BHs. The poor resolution close and inside the BH sphere of influence, and the simple thermodynamics used, prevent us from giving an estimate of the mass accretion rate on the horizon distance-scale. We can only speculate that in this phase the BH may accrete, generating a double nucleus AGN.

3.2 Eccentric orbits

We consider here the case of two equal mass BHs in the disc plane, the first moving on a initially circular orbit, and the second on an initially eccentric orbit ($e = 0.97$) with same binding energy (run B). Figure 5, upper panel, shows the BH distances from the centre of mass, as a function of time. We find that the sinking time of the eccentric BH is comparable to that of the companion, but what is remarkable is the strong effect of circularization seen in the orbit of the eccentric BH. Dynamical friction in a rotationally supported gaseous medium makes eccentric sinking orbits circular. This is opposite to what is found in isotropic, purely collisionless spherical backgrounds (Colpi, Mayer & Governato 1999, van den Bosch et al. 1999), or in a spherical pressure–supported gaseous background (Sanchez–Salcedo & Brandenburg 2000).

Figure 6 shows the density map of the gaseous disc viewed face–on. During the sinking process the BHs develop prominent wakes that are perturbing the underlying gas density. The BH moving initially on a circular orbit, spirals inwards maintaining its over-density behind its trail. The BH moving initially on the eccentric orbit undergoes instead a remarkably different evolution. Close to the pericentre (upper left panel) the eccentric BH has a speed larger, in modulus, than the local gas speed, and so its wake is excited behind its trail. The wake brakes the orbit and erodes the radial component of the velocity. On the other hand, around the apocentre the BH moves more slowly and its tangential velocity (which dominates over the radial, at this distance) is lower that the local rotational gas velocity. This causes the interesting fact, clearly illustrated in the upper right panel, that the wake is dragged in front of the BH, increasing its angular momentum. When approaching again pericentre, the wake tends to realign behind the BH, as shown in the two lower panels. The net effect highlighted in Figure 6 is the circularization of the BH orbit (see Figure 5, upper panel).

We have run a case without disc, letting the BHs sink under the action of the drag force due solely to the stellar bulge (run E).

As illustrated in Figure 7, we find that the inspiral takes a longer time compared to the case with gas, since the density of stars does not rise significantly (in a Plummer model), but, interestingly, the drag force does not lead to any circularization of the orbit, due to the lack of rotation in the

FIGURE 6

Figure 6. Time sequence of the sinking of the BHs, from run B. The panels show a face–on projection of the disc and BH positions at four different times. The color coding indicates the z–averaged gas density (in linear scale), and the white lines trace the BH counterclockwise prograde orbits. In the upper left panel the over–density created by both BHs are behind their current trail, while in the right upper panel, the BH moving on the eccentric orbit finds its own wake in front of its path. The wake is dragged by the faster rotation of the disc. In the two lower panels we observe a bending of the wake that tends to re–align, with time, behind the direction of motion of the BH.

background. Furthermore, we observe an increase in the eccentricity in the BH moving initially on a circular orbit, in line with the findings of Colpi et al. (1999).

As far as accretion is concerned, we notice that the BH moving along the initially eccentric orbit is unable to collect substantial gas mass in its vicinity, given its high velocity relative to the underlying background. Only when the orbit becomes circular the gathering of gas can occur (see Figure 5, lower panel). Thus, double nuclear activity does not

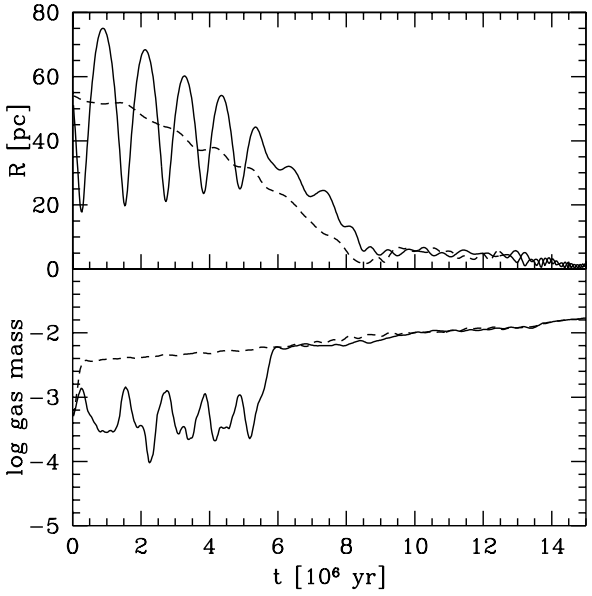

Figure 5. Upper panel: *Solid* (*dashed*) line shows the distance R (pc) of the eccentric (circular) BH from the centre of mass of the system as a function of time t. Lower panel: *Solid* (*dashed*) line shows the mass of the over-density in internal units (as defined in the text) corresponding to the eccentric (circular) BH as a function of time.

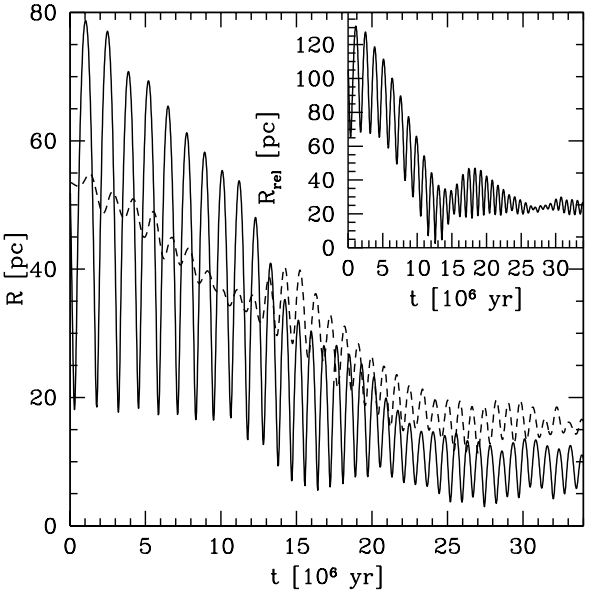

Figure 7. Distance R from the centre of mass, as a function of time t, for run E. In the simulation the sole collisionless bulge is considered. *Solid* (*dashed*) line refers to the BH set initially onto an prograde eccentric (circular) orbit. In the insert we give the relative orbital distance; axes are in the same units.

always set in, but instead it depends on the properties of the BH orbits.

When circularization is completed, the sinking process ends as in run A. Figure 8 shows the density map, in the plane of the BHs $z_{\rm BH}$, at the time the two BHs form a binary system, i.e., when the action of dynamical friction becomes inefficient; an over-density of ellipsoidal shape surrounds the binary, resulting from the superposition of the gravitational potentials of the two BHs.

4 DYNAMICS OF UNEQUAL MASS BLACK HOLES

Since merging galaxies may host BHs with different masses, in this Section, we explore the dynamics of two BHs with mass ratio 5:1 (see Table 1 for the details of the runs). The heavier BH has a mass $M_{\rm BH_1} = 0.05 M_{\rm Disc.}$

4.1 Circular orbits

We first explored the case in which the two BHs move initially on circular prograde orbits, at equal distances from the centre of mass (run C). The large, more massive BH sinks rapidly toward the centre of the gaseous disc, over a timescale of ~ 4 Myrs, as illustrated in Figure 9, while the lighter completes its orbital decay on a timescale longer by a factor $\simeq 2-3$. This implies that the dynamical friction time does not scale exactly as the inverse of the mass, and we interpret this result as an effect related to the perturbation in the overall disc gravitational potential caused by

FIGURE 8

Figure 8. Density profile in $z = z_{\rm BHs}$ plane at time 15 Myrs. Lines describe isodensity regions of $\rho = 0.25, 0.125, 0.09375$ and 0.0625 (in internal units). Black dots correspond to the two BH positions.

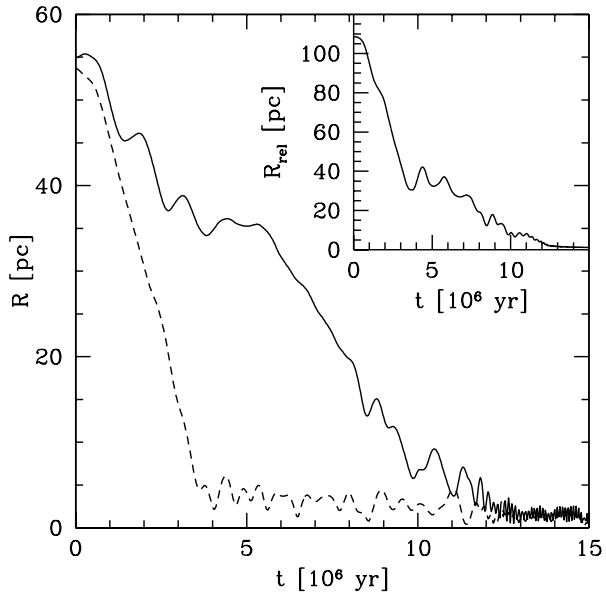

Figure 9. Same as Figure 3 for run C. *Solid* (*dashed*) line refers to the lighter (heavier) BH.

FIGURE 10

Figure 10. Same as Figure 6 for run C. In the upper panel ($t = 1$ Myr) the heavier BH perturbs the gaseous disc and shifts the barycentre of the system away from the lighter one. In the lower panel ($t = 3.5$ Myr), the heavier BH is located between the other BH and the barycentre, speeding up the orbital decay of the lighter one.

the larger BH. During the early stages, the two BHs are symmetrically displaced relative to the centre of mass, and start to develop their own wakes of different intensity. In the upper panel of Figure 10 we catch the instant at which the heavier BH, having perturbed the gaseous mass, causes a shift of the barycentre, i.e., a displacement in the direction opposite to the lighter BH. At this time, the orbital decay of the less massive BH halts temporarily (as shown also in Figure 9 between 3 and 6 Myrs). When the orbital decay of the heavy BH is sufficiently advanced that it has almost reached the centre, its location is in between the position of the lighter BH and the barycentre which is now shifted toward the light hole deepening the potential well. This causes an acceleration toward the disc centre speeding the orbital decay (see lower panel of Figure 10 and Figure 9 at times $\gtrsim$ 6 Myrs). This case illustrates that time variations in the underlying gravitational potential, that can be computed self–consistently in a real simulation, can modify granted dependences of the dynamical friction timescales. We find also that dynamical friction is effective until we hit the force resolution limit, and that no ellipsoidal density distribution is found (see §4.2 for a discussion).

Our initial condition is clearly arbitrary, and it is likely that in real mergers the heavier BH is already in place at the centre of the circum-nuclear disc by the time the second BH enters the disc. For this reason the sinking process may be different for the same BH masses involved, depending on the details of the process of paring. In the next simulation where the lighter BH is set onto an eccentric orbit, we allow the more massive hole to reach the centre before the sinking process of the light one takes place.

4.2 Eccentric orbits

In run D, the light BH is initially set on a prograde orbit with $e = 0.95$. Its sinking as a function of time proceeds, similarly to run B, with the circularization of the orbit. Since the larger BH is already in place at the centre of the gaseous disc we do not see any effect on the acceleration of the orbit besides dynamical friction. As shown in the upper panel of Figure 11 the orbit of the light hole becomes circular at a time $t \simeq 5$ Myrs. The evolution of the eccentricity is shown in Figure 12. In the early inspiral, the gas mass associated to the over-density in the neighborhood of the small BH is only $M_{\rm Gas} \sim 3 \times 10^{-3} M_{\rm BH_l}$, and only when the orbit becomes circular, we observe a rapid increase to a value $\sim 0.25 M_{\rm BH_l}$, potentially triggering an episode of accretion. When the light hole binds to the larger one ($t \simeq 11$ Myrs), it finds itself embedded inside the over-density created by the large hole, as shown in the lower panel of Figure 11. Contrary to the case of equal mass BHs, at very late times, the overdensity distribution around the binary BHs is not any longer ellipsoidal in shape and the gravitational field is weakly dipolar. Figure 13 shows how strong is the degree of sphericity of the gas surrounding the two BHs. Does orbital decay proceed further? The light BH seems to decay but at a much lower pace. The lack of a visible wake and the absence of an ellipsoidal deformation (torquing the binary components) suggest that the gas has become sufficiently stiff and the potential well sufficiently deep, due to the presence of the more massive hole, that orbital decay is halted or delayed.

In run F, we explore the dynamics of an unequal mass

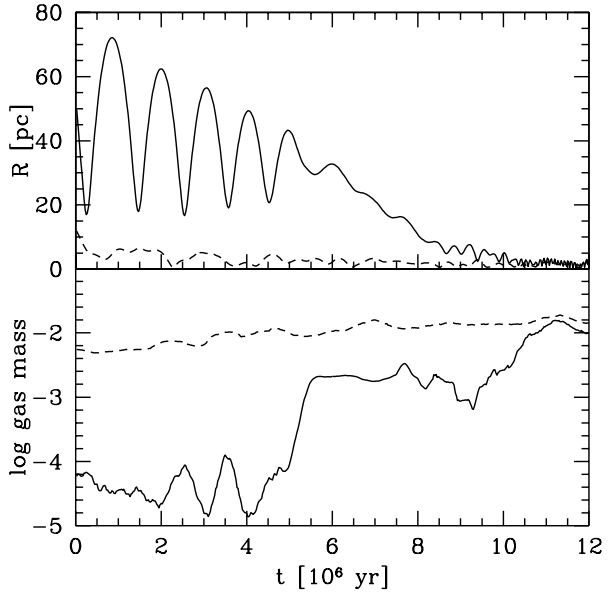

Figure 11. Upper panel: *Solid* (*dashed*) line shows the distance R (pc) of the lighter (heavier) BH from the centre of mass of the system as a function of time t. Lower panel: *Solid* (*dashed*) line shows the mass (in internal units)of the over-density corresponding to the lighter (heavier) BH as a function of time.

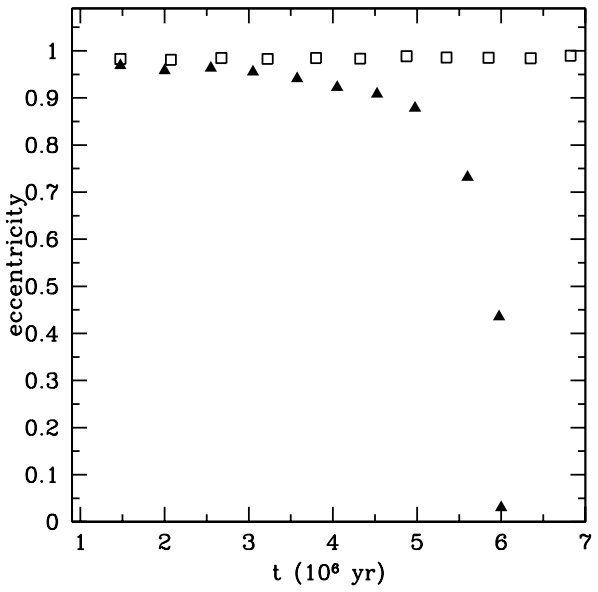

Figure 12. Eccentricity of the less massive BH as a function of time, in the case of prograde (Run D, *triangles*), and retrograde (Run F, *squares*) orbit. The eccentricity is computed over any half orbit.

BH set on a retrograde eccentric orbit. This is opposite to run D and is considered in order to bracket uncertainties in the way BHs bind. We find that the orbit remains eccentric (see Figure 12), preventing the gas to accumulate substantially around the BHs during the whole inspiral process. Given the rotational pattern of the gas, the over-density created by the BH stays always behind its trail, so that the eccentric BH does not circularize, as shown in figure 14. Note that the sinking time is about twice larger if compared to the prograde cases.

5 DISCUSSION

We explored the dynamics of a MBH pair orbiting inside a gaseous disc embedded in a spherical stellar distribution. We followed the slow inspiral of the pair, driven by dynamical friction, until the MBHs bind to form a close binary. The calculation is idealized in many ways, since we assumed a particular density distribution for the gas particles (Mestel disc), and neglected gas cooling and star formation.

Despite these limitations, we highlighted basic features of the dynamics of *LISA* double BHs in gas–rich discs. When a BH initially is moving on a highly eccentric co–rotating orbit, its eccentricity decreases significantly, contrary to what occurs when the background is spherical and collisionless (as shown in Figure 7; Colpi et al. 1999). Disc rotation is the key element of the circularization: near apocentre, where the angular velocity of the MBH is smaller than that of the disc, the density pattern, created by the MBH along its motion, is dragged in front of the BH itself enhancing its angular momentum. As a consequence the MBHs tend to form a close

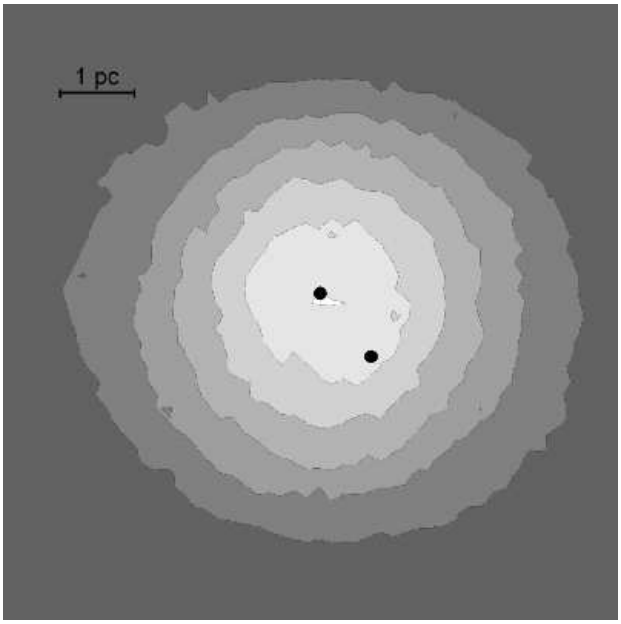

Figure 13. Same as Figure 8 for run D at time 13 Myr. The lines describe regions of $\rho = 2, 1, 0.5, 0.25, 0.125, 0.0625$ (in internal units). The isodensity contours are almost circular.

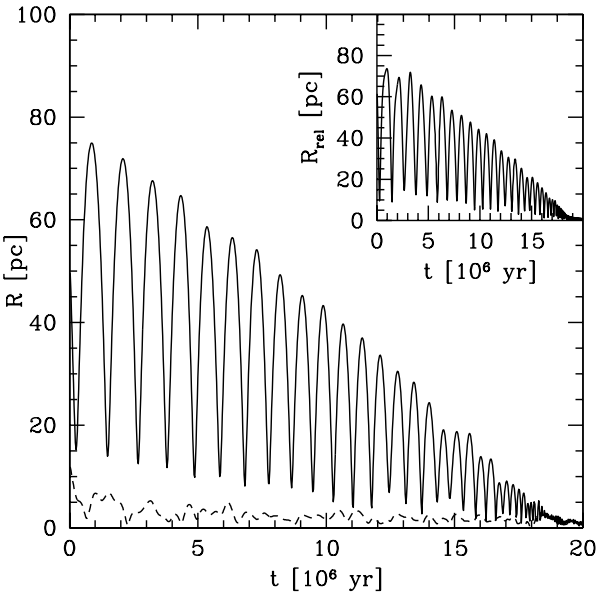

Figure 14. Same as Figure 3 for run F. *Solid* (*dashed*) line refers to the lighter (heavier) BH.

binary with a low eccentricity. However, the numerical noise at the end of the simulation does not allow us to calculate the precise value of any residual eccentricity. In the case of counter–rotating orbits, the eccentricity does not decrease since the density wake remains always behind the BH motion, and the MBHs may end forming a binary with still significant eccentricity (Figure 12). The probability of pairing along counter or co–rotating orbits is not known yet, and should be further investigated creating a statistically significant sample of simulations of gas–rich merging galaxies, similar to those carried out by Kazantzidis et al. (2005).

To summarize, if co–rotating orbits are more likely, we can note that the braking of MBHs in a gaseous background deliver a MBHB on a nearly circular orbit. It is worth noticing that, during later phases, further eccentricity evolution may still occur, driven by close encounters with single stars (Mikkola & Valtonen 1992, Quinlan 1996, Milosavljevic & Merritt 2001, Aarseth 2003, Berczik, Merritt & Spurzem 2005), and/or gas–dynamical processes (Armitage & Natarajan 2005), before GW emission acts to circularize the orbits. In Armitage & Natarajan (2005) the eccetricity is shown to grow substantially at very small separations, when gravitational torques from the MBHB act to clear a gap in the circum–binary disc. This fact may have important consequences for a possible final, GW driven, coalescence of the two BHs.

We find in addition, that when dynamical friction has subsided, in the case of equal mass BHs, the binary that forms is surrounded by gaseous particles belonging to the head of the wakes that merge in a coherent pattern, i.e., an ellipsoidal mass distribution. In the case of unequal masses, we observe on the contrary that the trailing over-density created by the light BH brings it to a closer distance from the heavier central BH. Given the large unbalance between the two masses, the gas distribution around the binary remains remarkably spherical and there is no gravitational torque in action to cause further inspiral of the light BH, within our resolution limit.

The feeding of BHs during their inspiral is also a key related issue. Despite the limitations of the thermodynamics employed, we have shown that a MBH moving on an eccentric orbit is unable to gather a relevant amount of gas in its vicinity, having a much higher velocity relative to the background. Only when the MBH orbit becomes nearly circular, gas is collected close by. This may conduct to the formation of an accretion disc fueling the MBH, hence triggering nuclear activity, observable on scales of a few pc, during the pairing. Then, AGN activity could be linked to the dynamics of the pairing process of the MBHs inside circum–nuclear discs. The possible presence of accretion discs near the horizons of coalescing MBHs is of particular importance, as it may leave an electromagnetic signal correlated the GW emission targeted by *LISA* (Armitage & Natarajan 2002, Milosavljevíc & Phinney 2005, Kocsis et al. 2005). We plan to improve upon our model, e.g., including gas cooling and heating, star formation, BH treated as sink particles, in order to explore the accretion issue in much greater detail.

Whether circularization stalls the *LISA* BHs to separations larger than critical for the intervention of GWs is not clear yet. The exploration of later stages requires a much higher force resolution and a modeling of the BHs as "absorbing" particles, having an horizon, i.e., a trapping surface. ELCM05 show, for two $M_{\rm BH} = 5 \times 10^7$ M$_\odot$, that the dynamical action of the torque continues at least down to a separation $\simeq 0.1$ pc, where the time to coalescence (because of gravitational wave emission) is about 10 Gyrs. However it is not clear if the process is still relevant for different conditions, not discussed by ELCM05, i.e., different disc–to–binary mass ratio, and/or different BH–BH mass ratio. We can just note that binary BHs in gaseous rotating background do not bind on those highly eccentric plunging orbits that would bring them straight to coalescence. *LISA* BHs form circular binaries and may need additional mechanisms for continuing their hardening process. Three–body encounters with low angular momentum bulge stars is a possibility (Mikkola & Valtonen 1992, Quinlan 1996), though it seems that BH binaries must be on highly eccentric orbits to drive the separation to sub-pc scales, where gravitational wave emission takes over (Sesana et al. 2005, in preparation). One aspect worth considering is that, during the hardening phase, one or both BHs could accrete gas, hence increase their mass, modifying the dynamics of the binary. Lets us now suppose that the mass of the member M_1 (M_2) of a circular binary increases by a factor β_1 (β_2). Then, if the binary angular momentum is conserved, we have a reduction of the binary separation by a factor

$$\frac{a_{\rm new}}{a_{\rm old}} = \frac{\beta_1 M_1 + \beta_2 M_2}{\beta_1^2 \beta_2^2 (M_1 + M_2)}. \quad (4)$$

As an example, let us consider a very unequal mass binary ($M_1 \gg M_2$): the heavier BH can indeed accrete while the secondary is slowly spiraling inwards, as in run D. From equation 4, an increase of M_1 by a factor of, say, 2, reduces the binary separation by the same factor. This is quite promising, as, in scattering experiments (Sesana et al. 2005, in preparation), *LISA* circular binaries tend to stall at sep-

arations which are factors $\sim 2-8$ (depending on mass and mass ratio) too large to drive the binary to coalesce within 1 Gyr because of gravitational wave emission.

ACKNOWLEDGMENTS

The authors thank Andres Escala, Lucio Mayer, Ruben Salvaterra, Javier Sanchez, Boris Sbarufatti and Alberto Sesana for fruitful comments and suggestions, and Franz Livio and Luca Paredi for technical support.

REFERENCES

Aarseth S.J., 2003, Ap&SS, 285, 367
Armitage P.J., Natarajan P., 2002, ApJ, 567, L9
Armitage P.J., Natarajan P., 2005, ApJ, in press (astro-ph/0508493)
Ballo L., Braito V., Della Ceca R., Maraschi L., Tavecchio F., Dadina M., 2004, ApJ, 600, 634
Begelman M.C., Blandford R.D., Rees M.J., 1980, Nature, 287, 307
Bender P. et al. , 1994, *LISA, Laser Interferometer Space Antenna for gravitational wave measurements*: ESA Assessment Study Report
Berczik P., Merritt D., Spurzem R., 2005 (astro-ph/0507260)
Colpi M., Mayer L., Governato F., 1999, ApJ, 525, 720
Colpi M., Possenti A., Gualandris A., 2002, ApJ, 570, 85
Downes D., Solomon P.M., 1998, ApJ, 507, 615
Escala A., Larson R.B., Coppi P.S., Maradones D., 2004, ApJ, 607, 765
Escala A., Larson R.B., Coppi P.S., Maradones D., 2005, ApJ, 630, 152 (ELCM05)
Ferrarese L., Merritt D., 2000, ApJ, 539, L9
Gebhardt K. et al. , 2000, AJ, 119, 1157
Gebhardt K., Rich R.M., Ho L.C., 2002, ApJ, 578, 41
Gebhardt K., Rich R.M., Ho L.C., 2005, ApJ, in press (astro-ph/0508251)
Gerssen J., van der Marel R.P., Gebhardt K., Guhathakurta P., Peterson R.C., Pryor C., 2002, AJ, 124, 3270
Governato F., Colpi M., Maraschi L., 1994, MNRAS, 271, 317
Häring N., Rix H.W., 2004, ApJ, 604, L89
Haenelt M.G., 1994, MNRAS, 269, 199
Hutchings J.B., Neff S.G., 1989, AJ, 97, 1306
Jaffe A.H., Backer D.C., 2003, ApJ, 583, 616
Kazantzidis S., Mayer L., Colpi M., Madau P., Debattista V.P., Wadsley J., Stadel J., Quinn T., Moore B., 2005, ApJ, 623, L67
Kocsis B., Frei Z., Haiman Z., Menou K., 2005, Apj, submitted (astro-ph/0505394)
Komossa S., Burwitz V., Hasinger G., Predehl P., Kaastra J.S., Ikebe Y., 2003, ApJ, 582, 15
Kormendy J., Richstone D., 1995, ARA&A, 33, 581
Magorrian J. et al. , 1998, AJ, 115, 2285
Makino J., Ebisuzaki T., 1996, ApJ, 465, 527
Makino J., Funato Y., 2004, ApJ, 602, 93
Mikkola S., Valtonen M.J., 1992, MNRAS, 259, 115
Miller M.C., Colbert E.J.M., 2004, IJMP, D13, 1-64
Milosavljević M., Merritt D., 2001, ApJ, 563, 34
Milosavljević M., Phinney E.S., 2005, ApJ, 622, 93
Ostriker E., 1999, ApJ, 513, 252
Quinlan G.D., 1996, NewA, 1, 255
Sanchez–Salcedo F.J., Brandenburg A., 2001, MNRAS, 322, 67
Sanders D.B., Mirabel I.F., 1996, ARA&A, 34, 749
Sesana A., Haardt F., Madau P., Volonteri M., 2005, ApJ, 623, 23
Sesana A., Haardt F., Madau P., 2005, in preparation
Shakura N.I., Sunyaev R.A., 1973, A&A, 24, 337
Soifer B.T. et al. , 1984, ApJ, 278, L71
Springel V., Yoshida N., White S.D.M., 2001, NewA, 6, 79
van den Bosch F.C., Lewis G.F., Lake G., Stadel J., 1999, ApJ, 515, 50
van der Marel R.P., Gerssen J., Guhathakurta P., Peterson R.C., Gebhardt K., 2002, AJ, 124, 3255
Volonteri M., Haardt F., Madau P., 2003, ApJ, 582, 559
Wada K., Norman C.A., 2001, ApJ, 546, 172
Yu Q., 2002, MNRAS, 331, 931

This figure "figure2.jpg" is available in "jpg" format from:

http://arXiv.org/ps/astro-ph/0509813v2

This figure "figure6.jpg" is available in "jpg" format from:

http://arXiv.org/ps/astro-ph/0509813v2

This figure "figure8.jpg" is available in "jpg" format from:

http://arXiv.org/ps/astro-ph/0509813v2

This figure "figure10.jpg" is available in "jpg" format from:

http://arXiv.org/ps/astro-ph/0509813v2